COVER SHEET

Raman spectroscopy of hydrotalcites with phosphate in the interlayer- implications for the removal of phosphate from water

Ray L. Frost•, Anthony W. Musumeci, J. Theo Kloprogge, Moses O. Adebajo and Wayde N. Martens

Inorganic Materials Research Program, School of Physical and Chemical Sciences, Queensland University of Technology, GPO Box 2434, Brisbane Queensland 4001, Australia.

Abstract

Hydrotalcites with phosphate in the interlayer were prepared at different pH. At pH >11.0 $(PO_4)^{3-}$ was the intercalated ionic species whereas at pH < 11.0 a mixture of $(PO_4)^{3-}$ and $(HPO_4)^{2-}$ ions was intercalated. Powder X-ray diffraction shows the hydrotalcite formed at pH 9.5 is poorly diffracting with a d-spacing of 11.9; whereas the d(003) spacing for the phosphate interlayered hydrotalcite formed at pH 11.9 and 12.5 were 8.0 and 7.9 Å. The addition of a thermally activated ZnAl-HT to a phosphate solution resulted in the uptake of the phosphate and the reformation of the hydrotalcite. Raman spectroscopy of the phosphate interlayered hydrotalcites shows the interlayered anion is pH dependent and only above pH 11.9 is the orthophosphate anion intercalated. At lower pH the monohydrogen phosphate anion is intercalated. Raman spectroscopy shows that upon addition of the thermally activated hydrotalcite to an aqueous phosphate solution results in the uptake of phosphate anion from the solution.

Key Words: hydrotalcite, brucite, phosphate removal, Raman microscopy, carrboydite, hydrohonessite, takovite, mountkeithite.

INTRODUCTION

Hydrotalcites, or layered double hydroxides (LDH's) are fundamentally anionic clays, and are less well-known as naturally occurring minerals than cationic clays like smectites [1,2]. The structure of hydrotalcite can be derived from a brucite structure ($Mg(OH)_2$) in which e.g. Al^{3+} or Fe^{3+} (pyroaurite-sjögrenite) substitutes a part of the Mg^{2+} [3-14]. This substitution creates a positive layer charge on the hydroxide layers, which is compensated by interlayer anions or anionic complexes [15,16]. Further mixtures of these mineral phases with multiple anions in the interlayer are observed. When LDH's are synthesized any appropriate anion including the phosphate anion can be placed in the interlayer. The hydrotalcite may be considered as a gigantic cation which is counterbalanced by anions in the interlayer. In hydrotalcites a broad range of compositions are possible of the type $[M^{2+}_{1-x}M^{3+}_x(OH)_2][A^{n-}]_{x/n}.yH_2O$, where M^{2+} and M^{3+} are the di- and trivalent cations in the octahedral positions within the hydroxide layers with x normally between 0.17 and 0.33. A^{n-} is an exchangeable interlayer anion [17]. In the hydrotalcites reevesite and pyroaurite, the divalent cations are Ni^{2+} and Mg^{2+} respectively with the trivalent cation being Fe^{3+}. In these cases, the carbonate anion is the major interlayer counter anion. Normally the hydrotalcite

• Author to whom correspondence should be addressed (r.frost@qut.edu.au)

structure based upon takovite (Ni,Al) and hydrotalcite (Mg,Al) has basal spacings of ~8.0 Å where the interlayer anion is carbonate. Reevesite and pyroaurite are based upon the incorporation of carbonate into the interlayer with d(001) spacings of around 8 Å [18,19].

There are many other important uses of hydrotalcites such as in the removal of environmental hazards in acid mine drainage [20,21], and a mechanism for the disposal of radioactive wastes [22]. Their ability to exchange anions presents a system for heavy metal removal from contaminated waters [23]. Structural information on different minerals has successfully been obtained recently by sophisticated thermal analysis techniques [6,24-28]. In this work we report the Raman spectroscopy of hydrotalcite with phosphate in the interlayer and explore the effect of pH on hydrotalcite formation. Further thermally activate hydrotalcites are used to remove phosphate from aqueous phosphate solutions.

EXPERIMENTAL

Synthesis of hydrotalcite compounds:

A mixed solution of aluminium and magnesium nitrates ($[Al^{3+}]$ = 0.25M and $[Mg^{2+}]$ = 0.75M; 1M = 1mol/dm^3) and a mixed solution of sodium hydroxide ($[OH^-]$ = 2M) and the desired anion either phosphate or carbonate, at the appropriate concentration, were placed in two separate vessels and purged with nitrogen for 20 minutes (all compounds were dissolved in freshly decarbonated water). The cationic solution was added to the anions via a peristaltic pump at 40mL/min and the pH maintained above 9. The mixture was then aged at 75°C for 18 hours under a N_2 atmosphere. The resulting precipitate was then filtered thoroughly with room temperature decarbonated water to remove nitrates and left to dry in a vacuum desiccator for several days. In this way hydrotalcites with different anions in the interlayer were synthesised. The phase composition was checked by X-ray diffraction and the chemical composition by EDX analyses.

Phosphate absorption

The hydrotalcite was heated at 255°C for 4 hours in order to destroy the 3-dimensional structure of the hydrotalcite and remove carbonate. The thermally activated powder (3.3g) was then placed in a large excess of decarbonated tri-sodium phosphate solution (0.1M, 350mL, pH ~ 12.5) and stirred under a Nitrogen atmosphere. Aliquots (50mL) were taken out at regular intervals, ensuring the nitrogen atmosphere was not disturbed. The resultant solution was vacuum filtered and rinsed once with freshly decarbonated water. The hydrotalcite was then left to dry in a vacuum desiccator to minimise exchange of phosphate ions in the interlayer for carbonate ions present in the air.

X-ray diffraction

X-Ray diffraction patterns were collected using a Philips X'pert wide angle X-ray diffractometer, operating in step scan mode, with Cu K_α radiation (1.54052 Å). Patterns were collected in the range 3 to 90° 2θ with a step size of 0.02° and a rate of

30s per step. Samples were prepared as a finely pressed powder into aluminium sample holders. The Profile Fitting option of the software uses a model that employs twelve intrinsic parameters to describe the profile, the instrumental aberration and wavelength dependent contributions to the profile.

Infrared spectroscopy

Infrared spectra were obtained using a Nicolet Nexus 870 FTIR spectrometer with a smart endurance single bounce diamond ATR cell. Spectra over the 4000–525 cm^{-1} range were obtained by the co-addition of 64 scans with a resolution of 4 cm^{-1} and a mirror velocity of 0.6329 cm/s. Spectra were co-added to improve the signal to noise ratio.

Raman microprobe spectroscopy

Hydrotalcite crystals were placed and orientated on a polished metal surface on the stage of an Olympus BHSM microscope, which is equipped with 10x and 50x objective lenses. The microscope is part of a Renishaw 1000 Raman microscope system, which also includes a monochromator, a filter system and a Charge Coupled Device (CCD). Raman spectra were excited by a Spectra-Physics model 127 He-Ne laser (633 nm) at a resolution of 2 cm^{-1} in the range between 100 and 4000 cm^{-1}. Repeated acquisition, using the highest magnification, was accumulated to improve the signal to noise ratio in the spectra. Spectra were calibrated using the 520.5 cm^{-1} line of a silicon wafer. Powers of less than 1 mW at the sample were used to avoid laser induced degradation of the sample [29-31]. Slight defocusing of the laser beam also assists in the preservation of the sample.

Spectroscopic manipulation such as baseline adjustment, smoothing and normalisation were performed using the Spectracalc software package GRAMS (Galactic Industries Corporation, NH, USA). Band component analysis was undertaken using the Jandel 'Peakfit' software package, which enabled the type of fitting function to be selected and allows specific parameters to be fixed or varied accordingly. Band fitting was done using a Gauss-Lorentz cross-product function with the minimum number of component bands used for the fitting process. The Gauss-Lorentz ratio was maintained at values greater than 0.7 and fitting was undertaken until reproducible results were obtained with squared correlations of r^2 greater than 0.995.

RESULTS AND DISCUSSION

X-ray diffraction of the thermally activated hydrotalcite and the phosphate adsorbed hydrotalcite

The X-ray diffraction patterns for the phosphate interlayered hydrotalcites are shown in Figure 1. Hydrotalcite normally has a d(003) spacing of 7.9 Å [32-35]. The sulphate interlayered hydrotalcite has a spacing of 8.0 Å. The XRD patterns show that the d-spacing for the phosphate interlayered hydrotalcite is pH dependent. The hydrotalcite formed at pH 9.3 shows a high degree of amorphicity. However the d(003) spacing can be still determined as 11.91 Å. The d-spacing for the pH=11.9 formed hydrotalcite is 8.04 Å and the value for the phosphate interlayered hydrotalcite at pH

12.5 is 7.9 Å. The d(003) spacing for the sulphate, chromate and molybdate interlayered hydrotalcites are 8.0, 7.9_8 and 7.9_7 Å respectively. Such values are close to the d-spacing values reported for the natural hydrotalcite with sulphate in the interlayer. The decreased interlayer spacing is attributed to the reduction in size of the hydrated phosphate anion between the brucite-like layers. Because of the uncertainty of the complete formation of the phosphate interlayered hydrotalcite formed at pH 9.3, the thermal decomposition was not studied further. The final products of the thermal decomposition of the carbonate interlayered hydrotalcite are MgO and $MgAl_2O_4$ (spinel). This observation means that the phosphate is lost during the thermal decomposition process.

The XRD patterns of the thermally activated carbonate interlayered hydrotalcite are shown in Figure 2. The XRD pattern of the hydrotalcite (top diffractogram in Figure 2) clearly shows the pattern of a typical hydrotalcite and may be compared with the reference pattern JCPDS 00-048-1025. A perfect match is observed. The hydrotalcite is thermally activated by heating to above the decomposition temperature of 265 °C. This temperature was chosen based upon the thermal analysis results. These results show that dehydration, dehydroxylation and loss of carbonate has occurred by this temperature. Figure 2 shows the XRD pattern of the thermally activated hydrotalcite and the pattern corresponds to that of ZnO. The thermal activation of the hydrotalcite results in the destruction of the layered structure.

Upon addition of the thermally activated hydrotalcite to an aqueous solution containing sodium phosphate the so-called 'memory' effect of hydrotalcites comes into play. Hydrotalcites after thermal decomposition will regain their original structure providing the compound is not heated to too high a temperature. This effect may be observed in Figure 2 where the XRD pattern of a hydrotalcite is restored after only thirty minutes. Additional peaks are observed and a large d-spacing of d(003) of 10.7 Å is observed for the first hour of exposure. A second d(003) spacing is observed at 7.6 Å. At the 1 hour exposure of the thermally activated ZnAl hydrotalcite two d(003) spacings of 10.6 and 7.5 Å are observed. The d-spacing of 10.6 Å is lost after 1 hour. At 2 hours the d(003) spacing is 7.527 Å and at 4 hours the spacing is 7.530 Å. The XRD pattern for the reformed hydrotalcite does not change on further exposure to the aqueous media. The d(003) spacing of 7.5 Å is observed.

Raman Spectroscopy

Upon formation of hydrotalcites with phosphates in the interlayer under different pH conditions, it is not known whether the phosphate in the interlayer is in the form of the triphosphate anion, the monohydrogen diphosphate anion or the dihydrogen phosphate anion. The Raman spectra of these anions are shown in Figure 3. The Raman spectra of the phosphate anions will alter as hydrogen is attached to the phosphate as the symmetry will change from T_d to C_{3v} to C_{2v}. This progression will result in the loss of degeneracy and additional bands will be observed. Figure 3 reflects this loss of symmetry and the observation of additional bands. The Raman spectra of the aqueous trisodium phosphate solution show a single intense band at 941 cm^{-1} with some asymmetry on the low wavenumber side. This asymmetry may be due to the presence of the disodium monohydrogen phosphate anion which shows a strong intensity at 935 cm^{-1}. There is an equilibrium between these two ions which

Raman spectroscopy readily picks up even though the concentration of the latter may be low. This equilibrium is shown as follows

$(PO_4)^{3-} + 3H^+ \Leftrightarrow (HPO_4)^{2-} + 2H^+ \Leftrightarrow (H_2PO_4)^- + H^+ \Leftrightarrow H_3PO_4$

The pH of the first step is 12.3, for the second 7.2 and the third 2.2. Thus at the pH used in the synthesis of the hydrotalcites used in this step, only the first two anions would be expected to be found in the hydrotalcite layers.

S. D. Ross in Farmer and references cited therein report the $(PO_4)^{3-}$ ν_1 symmetric stretching mode at 938 cm^{-1} based upon infrared data [36]. Two bands are observed in the spectra of the aqueous solution of the trisodium phosphate anion at 1033 and 1013 cm^{-1}. These bands are attributed to the $(PO_4)^{3-}$ antisymmetric stretching vibrations. In the spectrum of the monosodium dihydrogen phosphate an intense band is observed at 935 cm^{-1} with a second band at 1065 cm^{-1} and additional low intensity bands at 1002 and 858 cm^{-1}. S.D Ross in Farmer reported the ν_1 symmetric stretching mode for the disodium hydrogen phosphate at 860 cm^{-1} and the ν_3 modes at 1150, 1068 and 948 cm^{-1} [36]. In the Raman spectrum of the monosodium dihydrogen phosphate three bands are observed at 993, 944 and 914 cm^{-1}. Whilst there have been some infrared studies of phosphate interlayered hydrotalcites, there have been no Raman spectroscopic studies [37-40]. Adsorption of $(HPO_4)^{2-}$ ions on a nitrate hydrotalcite resulted in characteristic infrared bands between 1057 and 1064 cm^{-1} [41]. At high phosphate concentrations two additional bands observed as shoulders were found at 1120 and 990 cm^{-1}. The infrared spectrum of free monohydrogen phosphate anions gave bands between 1064 and 1067 cm^{-1} as well as 988 cm^{-1} [37,39,42]. Thus a comparison of the two sets of data shows that the anion is held between the hydrotalcite layers electrostatically and is not bonded to the hydrotalcite surface. In the latter situation a molecular arrangement such as $(MO)PO_2(OH)$ would be formed. The spectroscopy of this unit would be very different from the free phosphate anions. Badreddine et al. in a series of papers reported the infrared spectra as well as the PXRD spectra of Zn/Al LDH's [37,39]. Raman spectra of free phosphate oxyanions as in aqueous solutions show a symmetric stretching mode (ν_1) at 938 cm^{-1}, the antisymmetric stretching mode (ν_3) at 1017 cm^{-1}, the symmetric bending mode (ν_2) at 420 cm^{-1} and the ν_4 mode at 567 cm^{-1} and $(HPO_4)^{2-}$ ions display bands at 1005 (ν_1), 917 (ν_2), 1080 (ν_3) and 535 cm^{-1} (ν_4). The results reported by Badreddine et al. are not in agreement with the results reported in this work.

The Raman spectra of the hydrotalcites formed at different pH are shown in Figure 4. The results of the band component analyses of these spectra are reported in Table 1. The spectra show striking similarity. The phosphate interlayered hydrotalcite prepared at pH 12.5 shows two bands: an intense sharp band at 960 cm^{-1} and a broader band at 1026 cm^{-1}. These bands ate attributed to the $(PO_4)^{3-}$ symmetric and antisymmetric stretching vibrations. The spectrum is identical to that of the $(PO_4)^{3-}$ ion. The phosphate interlayered hydrotalcite prepared at pH 11.9 shows two bands: an intense sharp band at 957 cm^{-1} and a broader band at 1032 cm^{-1}. Additional bands are observed at 1394 and 1650 cm^{-1}. It is not known what the first band may be attributed to but one possibility is to a MOH deformation vibration. The second band is readily ascribed to a water Raman active bending mode. The band is not observed in the non-diffracting hydrotalcite formed at pH 9.3. This may simply indicate that the hydrotalcite has not been formed. For the phosphate interlayered hydrotalcite

prepared at pH 9.3, four bands are observed at 964, 989, 1033 and 1138 cm^{-1}. In aqueous systems the $(PO_4)^{3-}$ ion has an intense band at 936 cm^{-1}, whereas the Raman spectrum of the aqueous solution of the $(HPO_4)^{2-}$ anion shows an intense band at 990 cm^{-1}. In contrast the Raman spectrum of the $(H_2PO_4)^{-}$ anion shows three bands at 1077, 995 and 878 cm^{-1}; the latter being the most intense. Thus it is apparent there are two sets of overlapping bands: one set corresponding to the $(PO_4)^{3-}$ anion (964 and 1033 cm^{-1}) and a second set due to the $(HPO_4)^{2-}$ ion (989 and 1138 cm^{-1}). Thus it is concluded that the effect of pH on the formation of the phosphate interlayered hydrotalcite is that the $(PO_4)^{3-}$ species is interlayered at high pH whereas it is a mixture of the two anions [$(PO_4)^{3-}$ and $HPO_4)^{2-}$] which is interlayered at pHs between 11.9 and 12.3. It is probable that no LDH is formed at pH 9.3 as is evidenced by both XRD and Raman spectroscopy.

The Raman spectra of the phosphate interlayered hydrotalcites formed at pHs of 9.3, 11.9 and 12.5 pH units in the low wavenumber region are shown in Figure 5. The orthophosphate anion is tetrahedral with T_d symmetry, thus there are four normal modes of vibration, all of which are Raman active. However only the triply degenerate $\nu_3(F_2)$ and $\nu_4(F_2)$ modes are infrared active. The Raman spectrum of the oxyanion $(PO_4)^{3-}$ shows a symmetric stretching mode (ν_1) at 938 cm^{-1}, the antisymmetric stretching mode (ν_3) at 1017 cm^{-1}, the symmetric bending mode (ν_2) at 420 cm^{-1} and the ν_4 mode at 567 cm^{-1}. Figure 5 displays a strong band around 474 cm^{-1} which is assigned to the E bending mode of the $(PO_4)^{3-}$ ion. The band is at 474 cm^{-1} for the phosphate interlayered hydrotalcite formed at pH 12.5, 472 cm^{-1} at pH 11.9 and a broad band centred on 441 cm^{-1} at pH 9.3. According to S.D. Ross in Farmer (p393) the $(PO_4)^{3-}$ anion shows a ν_2 mode at 350 cm^{-1}. A broad feature is observed at 371 cm^{-1} for phosphate interlayered hydrotalcite formed at pH 12.5, 383 cm^{-1} at pH 11.9 and 334 cm^{-1} at pH 9.3. An additional intense band is observed at around 237 cm^{-1}. The infrared band expected at around 576 cm^{-1} is not observed in the Raman spectrum.

The Raman spectra of the thermally activated $ZnAlCO_3$ hydrotalcite exposed to aqueous phosphate solutions are shown in Figure 6. After half an hour contact two bands are observed at 961 and 932 cm^{-1}. These bands are attributed to the $(HPO_4)^{2-}$ and $(PO_4)^{3-}$ PO stretching modes. The bands are observed at 974 and 934 cm^{-1} after 1 hour exposure. After 2 hours exposure the band is observed at 959 cm^{-1} and further increases in time of exposure does not result in any changes in position. Associated with the PO stretching vibrations is a low intensity band at 1047 cm^{-1} which may be attributed to the ν_3 antisymmetric stretching vibration. A band appears in or around this position in all of the spectra. A band is observed at 1061 cm^{-1} in all the spectra and is assigned to the presence of carbonate. Even though the phosphate solutions were made carbonate free, the hydrotalcites still adsorb carbon dioxide probably from the atmosphere through some solid state reaction. Nevertheless the experiment shows that thermally activated hydrotalcite can be used to remove phosphate from an aqueous phosphate solution.

CONCLUSIONS

This research has shown that

a) Phosphate can be intercalated into a hydrotalcite as the counter anion.
b) This intercalation is pH dependent
c) The pH determines the nature of the anion in the interlayer
d) Thermally activated hydrotalcite can be used to remove phosphate from an aqueous system.
e) Raman spectroscopy identified the nature of the phosphate anion in the interlayer
f) Raman spectroscopy identified the nature of the anion in the reformed thermally activated hydrotalcite

Acknowledgments

The financial and infra-structure support of the Queensland University of Technology Inorganic Materials Research Program is gratefully acknowledged. The Australian Research Council (ARC) is thanked for funding.

References

1. Hashi, K, Kikkawa, S, Koizumi, M. *Clays and Clay Minerals* 1983**; 31**: 152.
2. Ingram, L, Taylor, HFW. *Mineralogical Magazine and Journal of the Mineralogical Society (1876-1968)* 1967**; 36**: 465.
3. Kloprogge, JT, Hickey, L, Frost, RL. *Materials Chemistry and Physics* 2005**; 89**: 99.
4. Frost Ray, L, Erickson Kristy, L. *Spectrochimica acta. Part A, Molecular and biomolecular spectroscopy* 2005**; 61**: 51.
5. Erickson, KL, Bostrom, TE, Frost, RL. *Materials Letters* 2004**; 59**: 226.
6. Frost, RL, Erickson, KL. *Journal of Thermal Analysis and Calorimetry* 2004**; 76**: 217.
7. Frost, RL, Erickson, KL. *Thermochimica Acta* 2004**; 421**: 51.
8. Kloprogge, JT, Hickey, L, Frost, RL. *Journal of Raman Spectroscopy* 2004**; 35**: 967.
9. Kloprogge, JT, Hickey, L, Frost, RL. *Journal of Solid State Chemistry* 2004**; 177**: 4047.
10. Frost, RL, Ding, Z. *Thermochimica Acta* 2003**; 405**: 207.
11. Frost, RL, Martens, W, Ding, Z, Kloprogge, JT. *Journal of Thermal Analysis and Calorimetry* 2003**; 71**: 429.
12. Frost, RL, Weier, ML, Clissold, ME, Williams, PA. *Spectrochimica Acta, Part A: Molecular and Biomolecular Spectroscopy* 2003**; 59**: 3313.
13. Frost, RL, Weier, ML, Clissold, ME, Williams, PA, Kloprogge, JT. *Thermochimica Acta* 2003**; 407**: 1.
14. Frost, RL, Weier, ML, Kloprogge, JT. *Journal of Raman Spectroscopy* 2003**; 34**: 760.
15. Taylor, RM. *Clay Minerals* 1982**; 17**: 369.
16. Taylor, HFW. *Mineralogical Magazine and Journal of the Mineralogical Society (1876-1968)* 1969**; 37**: 338.
17. Hansen, HCB, Koch, CB. *Applied Clay Science* 1995**; 10**: 5.
18. Bish, DL, Livingstone, A. *Mineralogical Magazine* 1981**; 44**: 339.
19. Nickel, EH, Clarke, RM. *American Mineralogist* 1976**; 61**: 366.
20. Lichti, G, Mulcahy, J. *Chemistry in Australia* 1998**; 65**: 10.
21. Seida, Y, Nakano, Y. *Journal of Chemical Engineering of Japan* 2001**; 34**: 906.
22. Roh, Y, Lee, SY, Elless, MP, Foss, JE. *Clays and Clay Minerals* 2000**; 48**: 266.
23. Seida, Y, Nakano, Y, Nakamura, Y. *Water Research* 2001**; 35**: 2341.
24. Horvath, E, Kristof, J, Frost, RL, Heider, N, Vagvoelgyi, V. *Journal of Thermal Analysis and Calorimetry* 2004**; 78**: 687.
25. Frost, RL, Weier, ML, Erickson, KL. *Journal of Thermal Analysis and Calorimetry* 2004**; 76**: 1025.
26. Frost, RL, Erickson, KL. *Journal of Thermal Analysis and Calorimetry* 2004**; 78**: 367.
27. Horvath, E, Kristof, J, Frost, RL, Redey, A, Vagvolgyi, V, Cseh, T. *Journal of Thermal Analysis and Calorimetry* 2003**; 71**: 707.
28. Kristof, J, Frost, RL, Kloprogge, JT, Horvath, E, Mako, E. *Journal of Thermal Analysis and Calorimetry* 2002**; 69**: 77.

29. Martens, W, Frost, RL, Kloprogge, JT, Williams, PA. *Journal of Raman Spectroscopy* 2003**; 34**: 145.
30. Frost, RL, Martens, W, Kloprogge, JT, Williams, PA. *Journal of Raman Spectroscopy* 2002**; 33**: 801.
31. Frost, RL, Martens, WN, Williams, PA. *Journal of Raman Spectroscopy* 2002**; 33**: 475.
32. Kloprogge, JT, Frost, RL. *Journal of Solid State Chemistry* 1999**; 146**: 506.
33. Kloprogge, JT, Frost, RL. *Tijdschrift voor Klei, Glas en Keramiek* 2000**; 21**: 7.
34. Ruan, HD, Frost, RL, Kloprogge, JT, Duong, L. *Spectrochimica Acta, Part A: Molecular and Biomolecular Spectroscopy* 2002**; 58**: 265.
35. Kloprogge, JT, Wharton, D, Hickey, L, Frost, RL. *American Mineralogist* 2002**; 87**: 623.
36. Farmer, VC *Mineralogical Society Monograph 4: The Infrared Spectra of Minerals*, 1974.
37. Badreddine, M, Legrouri, A, Barroug, A, De Roy, A, Besse, J-P. *Collection of Czechoslovak Chemical Communications* 1998**; 63**: 741.
38. Badreddine, M, Khaldi, M, Legrouri, A, Barroug, A, Chaouch, M, De Roy, A, Besse, JP. *Materials Chemistry and Physics* 1998**; 52**: 235.
39. Badreddine, M, Legrouri, A, Barroug, A, De Roy, A, Besse, JP. *Materials Letters* 1999**; 38**: 391.
40. Costantino, U, Casciola, M, Massinelli, L, Nocchetti, M, Vivani, R. *Solid State Ionics* 1997**; 97**: 203.
41. Hansen, HCB. *Clays Controlling the Environment, Proceedings of the International Clay Conference, 10th, Adelaide, July 18-23, 1993* 1995: 201.
42. Legrouri, A, Badreddine, M, Barroug, A, De Roy, A, Besse, JP. *Journal of Materials Science Letters* 1999**; 18**: 1077.

Phosphate pH = 12.5			Phosphate pH = 11.9			Phosphate pH = 9.3		
Centre	**FWHM**	**%**	**Centre**	**FWHM**	**%**	**Centre**	**FWHM**	**%**
			3688	52.1	1.57	**3677**	66.4	1.1
3639	116.3	9.6	**3628**	108.1	3.12			
						3607	119.4	2.0
3520	200.7	20.1						
			3494	226.6	26.57			
						3464	224.9	21.9
3349	306.6	40.4						
			3274	354.6	36.04	**3253**	365.9	51.3
3069	344.2	17.2						
			2969	280.8	9.42			
						2923	192.4	7.5
			2330	4.0	0.085			
1649	87.9	0.3	**1649**	104.3	0.82	**1649**	87.9	0.55
1394	96.2	0.9	**1391**	101.0	1.82			
						1129	61.9	0.69
1063	9.8	1.6	**1063**	13.0	2.48			
1050	7.6	1.2	**1048**	7.3	2.70			
1026	70.3	0.9	**1032**	70.8	1.97	**1032**	103.3	2.2
						989	40.3	2.5
960	52.9	1.5	**957**	67.9	3.38	**964**	29.0	2.4
706	25.8	0.1	**712**	28.9	0.20			
						627	40.3	0.26
			589	53.8	0.48			
552	24.4	3.3	**552**	26.1	2.69	**569**	75.2	2.1
474	38.5	0.8	**471**	51.1	2.46	**486**	47.0	0.28
						440	113.5	1.3
371	144.5	1.1	**383**	102.6	1.67			
						334	121.2	1.3
			305	69.5	0.62			
295	27.9	0.1						
237	61.4	0.5	**237**	58.6	1.23	**240**	67.2	1.4
197	29.0	0.3	**197**	28.9	0.59	**197**	26.7	0.69

Table 1 Results of the Raman spectral analysis of hydrotalcite intercalated with phosphate at pH 9.3, 11.9, and 12.9

$ZnAlPO_4$ Hydrotalcite (0.5 hour)			$ZnAlPO_4$ Hydrotalcite (1 hour)			$ZnAlPO_4$ Hydrotalcite (2 hour)			$ZnAlPO_4$ Hydrotalcite (4 hour)			$ZnAlPO_4$ Hydrotalcite (6 hour)		
Centre	**FWHM**	**%**	**Centre**	**FWHM**	**%**	**Centre**	**FWHM**	**%**	**Centre**	**FWHM**	**%**	**Centre**	**FWHM**	**%**
3755	72.3	0.9	**3753**	82.8	1.5	**3740**	149.0	17.7						
3582	67.2	4.8	**3584**	57.0	5.1				**3577**	73.0	5.2			
						3558	181.4	17.5				**3558**	77.5	4.7
3498	138.5	30.8	**3502**	134.3	28.8				**3503**	132.9	26.3	**3488**	138.5	28.6
						3447	116.8	7.4						
3410	117.2	13.4	**3422**	102.4	14.1				**3411**	130.1	18.8			
												3385	192.0	17.8
3345	153.4	11.0	**3346**	114.6	8.0									
									3323	182.2	13.7			
1421	56.2	0.2	**1405**	88.2	1.0							**1417**	94.8	2.3
						1138	65.3	2.6				**1155**	62.7	1.5
1071	50.9	1.3				**1072**	48.2	5.2						
1061	10.9	2.9	**1061**	11.2	2.6	**1061**	12.5	1.6	**1060**	9.9	2.3	**1060**	11.8	2.1
1047	11.8	0.4	**1050**	48.7	1.9	**1047**	9.2	0.4	**1055**	36.9	2.4	**1057**	95.7	5.3
1005	124.2	5.0				**1023**	43.0	1.4	**1014**	31.9	0.6			
			977	60.6	2.8									
961	42.4	1.6				**959**	62.6	6.8	**957**	62.8	3.5	**958**	57.9	4.5
932	36.1	1.6	**934**	35.3	1.9									
574	27.8	1.4				**578**	56.9	5.4				**576**	56.1	4.0
551	18.0	6.5	**551**	17.9	7.1	**551**	27.0	3.4	**552**	21.5	4.9	**551**	24.9	3.6
			541	105.6	4.1				**538**	100.8	3.6			
496	140.5	6.6	**489**	23.3	2.0	**494**	73.7	8.5	**491**	27.1	2.0	**496**	40.1	2.5
491	19.0	1.2												
437	9.3	0.4	**438**	10.4	0.3	**438**	12.6	1.8	**438**	15.7	0.3	**437**	10.8	1.2
			410	201.5	13.6	**416**	70.0	9.0	**410**	256.3	12.1	**415**	163.5	17.3
360	124.2	3.5												
						340	75.9	3.8				**330**	41.8	0.6
251	60.3	3.1	**260**	38.9	1.6	**246**	70.0	4.6	**258**	41.6	1.2	**259**	49.3	1.8

			229	33.7	0.8				**225**	28.3	0.9	**231**	39.1	1.0
200	26.7	3.4	**204**	17.4	2.0	**198**	26.4	2.9	**203**	18.0	1.4	**203**	21.4	0.9
			190	19.3	1.0				**189**	19.5	0.7	**191**	16.5	0.3

Table 2 Results of the Raman spectral analysis of thermally activated hydrotalcite exposed to phosphate solution as a function of time

LIST OF FIGURES

LIST OF TABLES

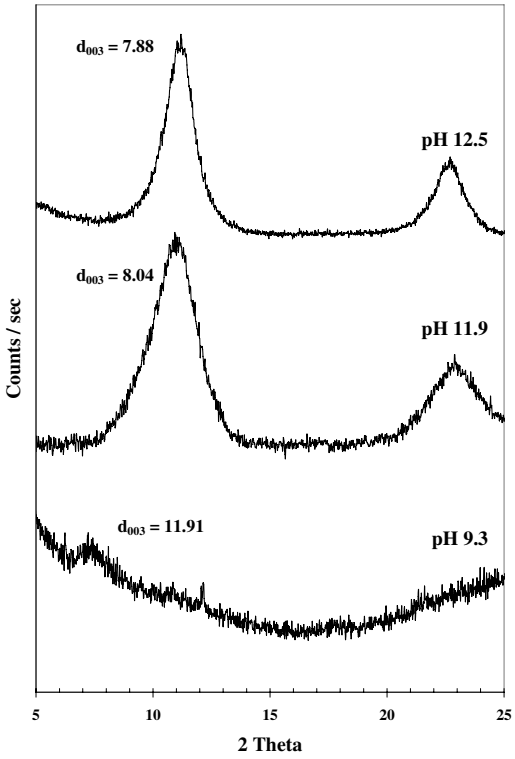
d_{003} = 7.88
pH 12.5
d_{003} = 8.04
pH 11.9
d_{003} = 11.91
pH 9.3
Counts / sec
5
10
15
20
25
2 Theta

Figure 1

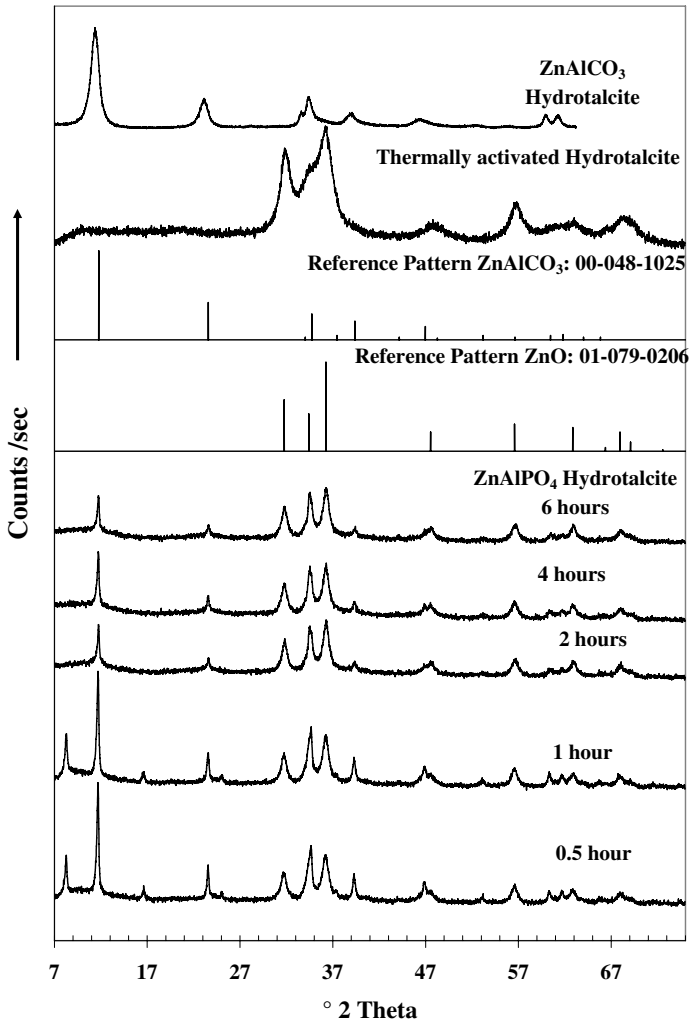
ZnAlCO3
Hydrotalcite
Thermally activated Hydrotalcite
Reference Pattern ZnAlCO3: 00-048-1025
Reference Pattern ZnO: 01-079-0206
ZnAlPO4 Hydrotalcite
6 hours
4 hours
2 hours
1 hour
0.5 hour
Counts /sec
7
17
27
37
47
57
67
° 2 Theta

Figure 2

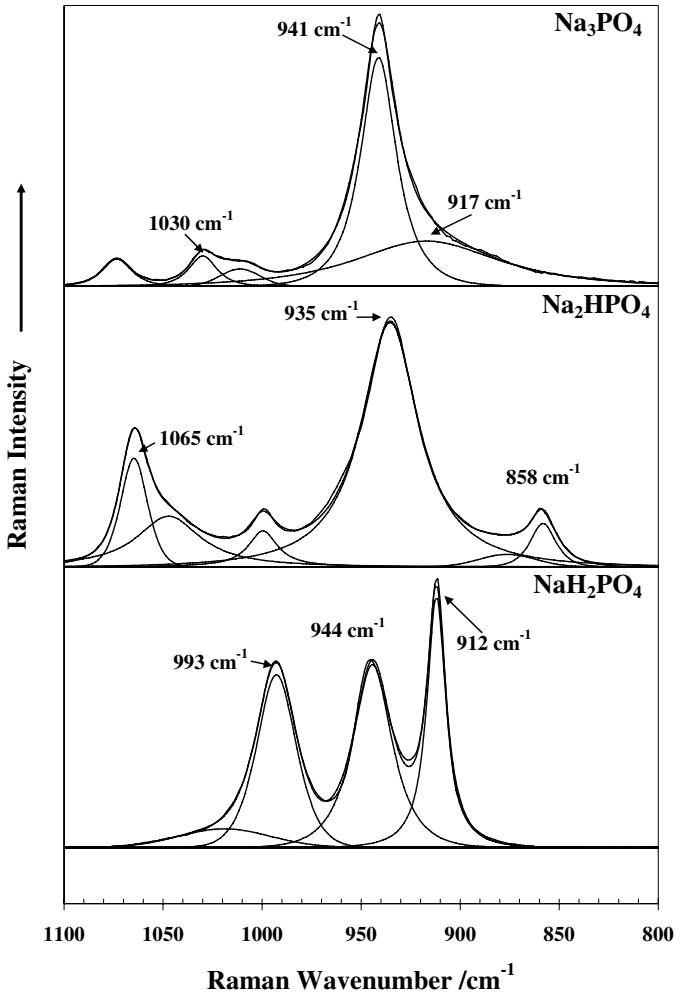
941 cm-1
Na3PO4
1030 cm-1
917 cm-1
935 cm-1
Na2HPO4
1065 cm-1
858 cm-1
NaH2PO4
944 cm-1
912 cm-1
993 cm-1
Raman Intensity
1100
1050
1000
950
900
850
800
Raman Wavenumber /cm-1

Figure 3

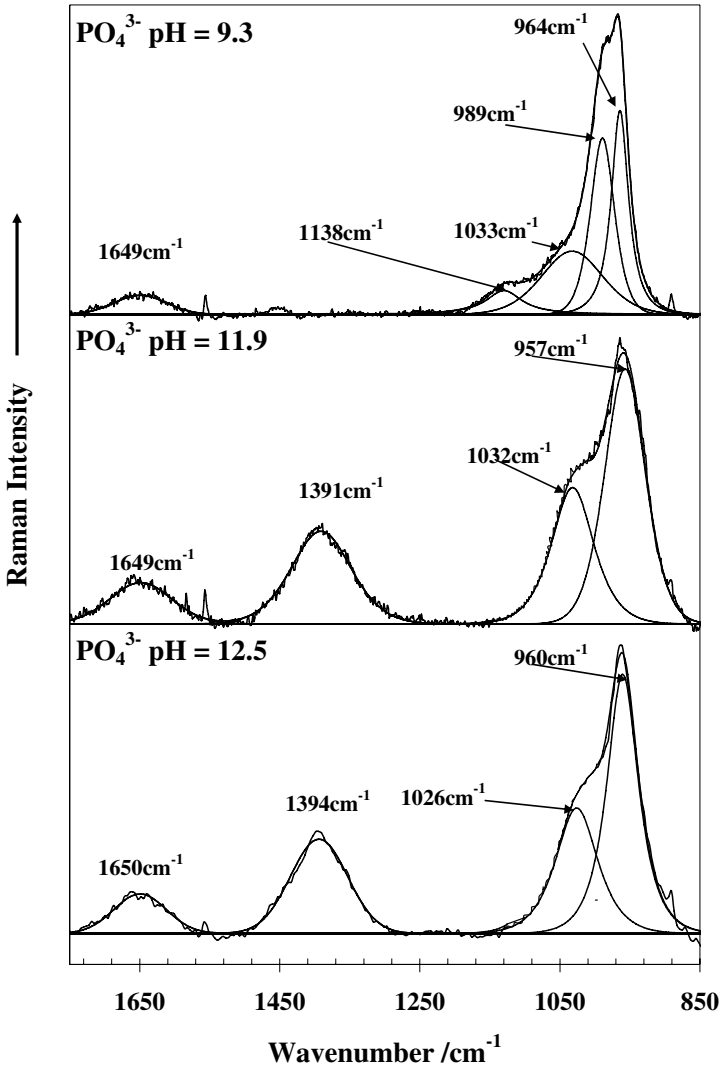
PO4 3- pH = 9.3
964cm-1
989cm-1
1649cm-1
1138cm-1
1033cm-1
PO4 3- pH = 11.9
957cm-1
1032cm-1
1391cm-1
1649cm-1
PO4 3- pH = 12.5
960cm-1
1394cm-1
1026cm-1
1650cm-1
Raman Intensity
1650
1450
1250
1050
850
Wavenumber /cm-1

Figure 4

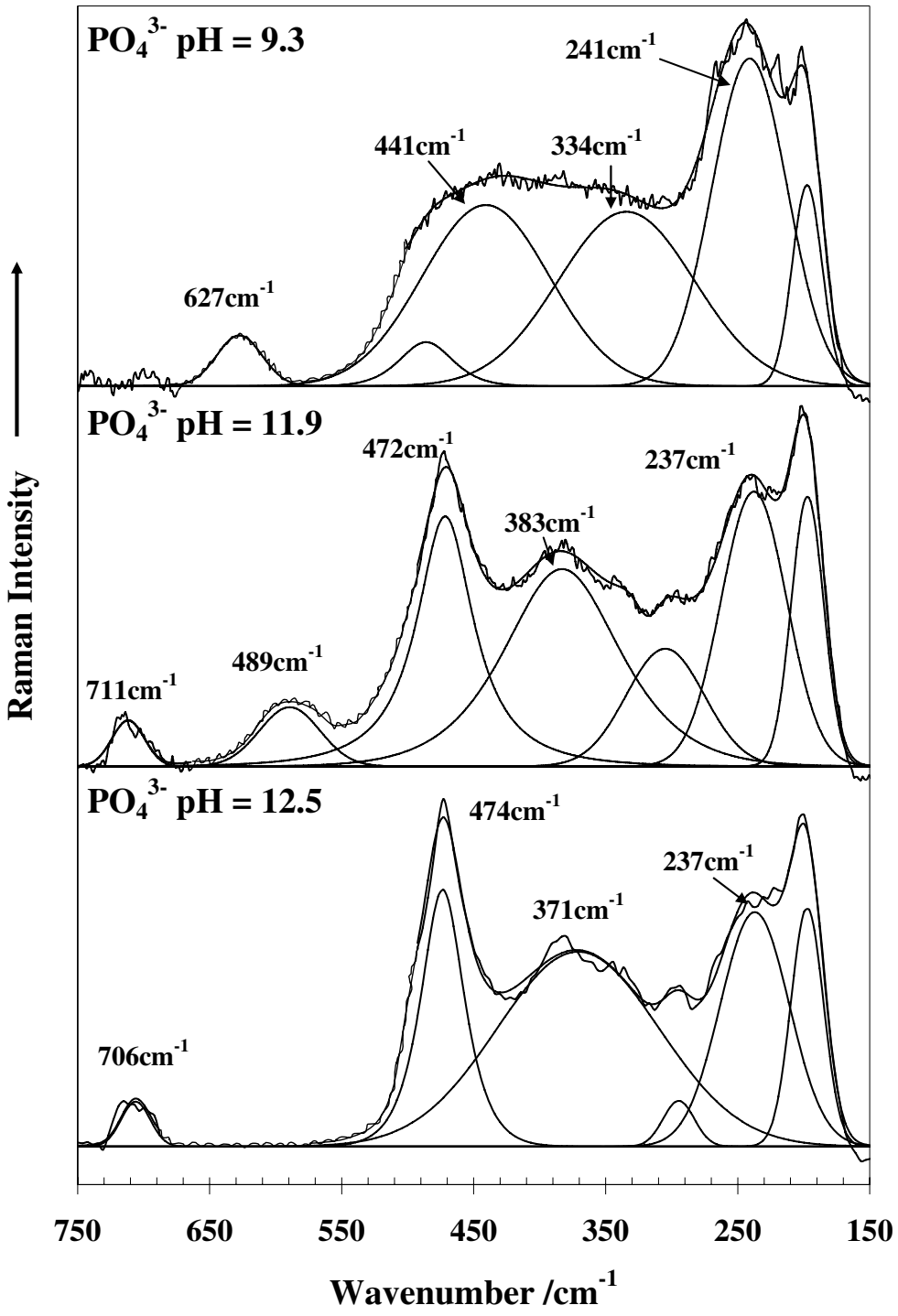
PO4 3- pH = 9.3
241cm-1
441cm-1
334cm-1
627cm-1
PO4 3- pH = 11.9
472cm-1
237cm-1
383cm-1
489cm-1
711cm-1
PO4 3- pH = 12.5
474cm-1
237cm-1
371cm-1
706cm-1
Raman Intensity
750
650
550
450
350
250
150
Wavenumber /cm-1

Figure 5

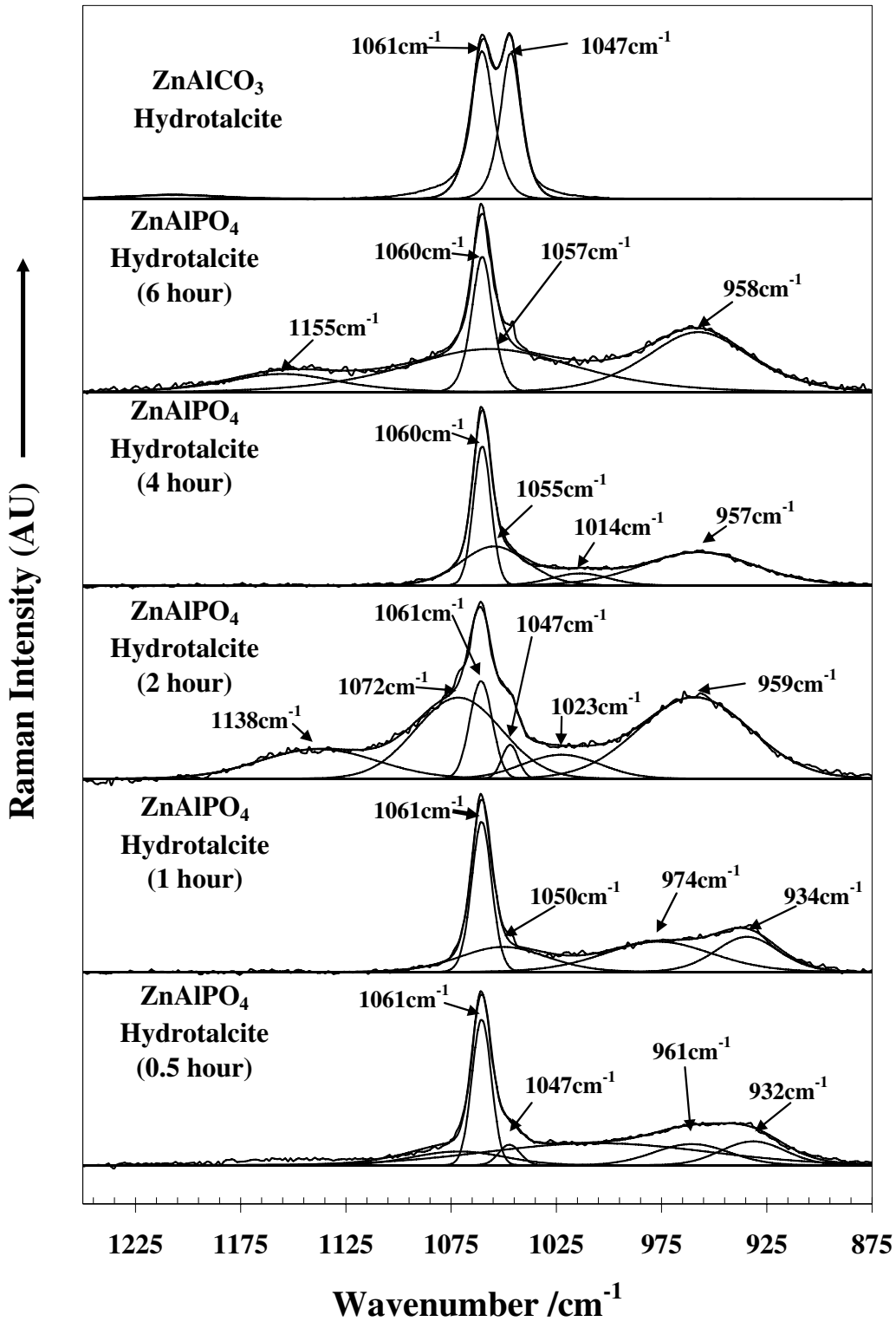
ZnAlCO3 Hydrotalcite
1061cm-1
1047cm-1
ZnAlPO4 Hydrotalcite (6 hour)
1060cm-1
1057cm-1
958cm-1
1155cm-1
ZnAlPO4 Hydrotalcite (4 hour)
1060cm-1
1055cm-1
1014cm-1
957cm-1
ZnAlPO4 Hydrotalcite (2 hour)
1061cm-1
1047cm-1
1072cm-1
959cm-1
1023cm-1
1138cm-1
ZnAlPO4 Hydrotalcite (1 hour)
1061cm-1
974cm-1
1050cm-1
934cm-1
ZnAlPO4 Hydrotalcite (0.5 hour)
1061cm-1
961cm-1
1047cm-1
932cm-1
Raman Intensity (AU)
1225
1175
1125
1075
1025
975
925
875
Wavenumber /cm-1

Figure 6

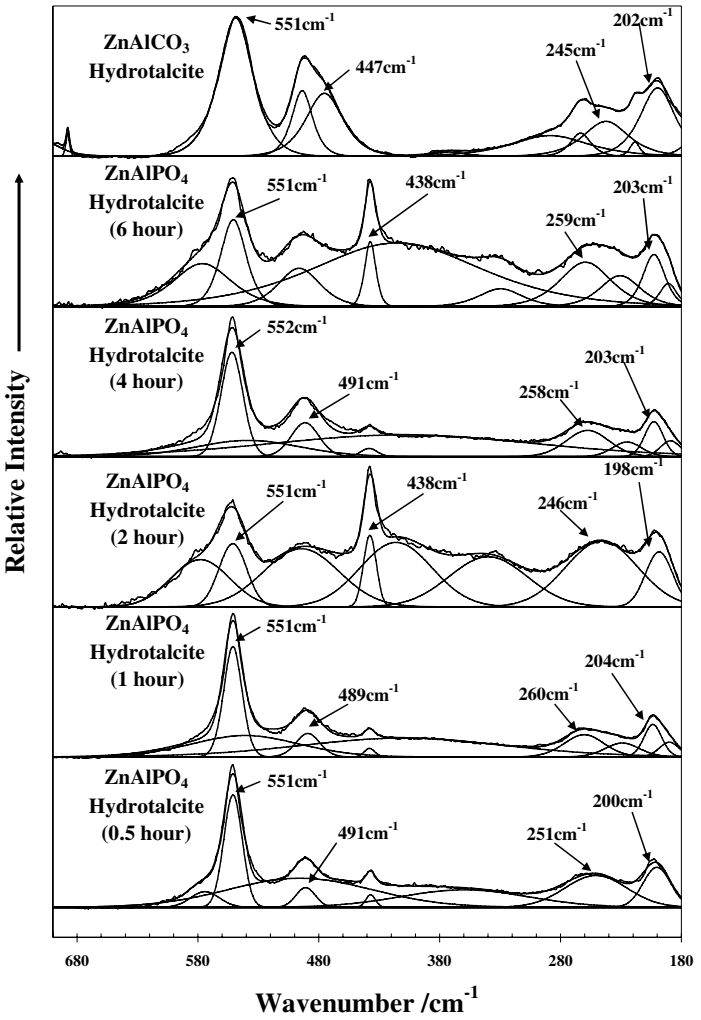
ZnAlCO3 Hydrotalcite
551cm-1
447cm-1
245cm-1
202cm-1
ZnAlPO4 Hydrotalcite (6 hour)
551cm-1
438cm-1
259cm-1
203cm-1
ZnAlPO4 Hydrotalcite (4 hour)
552cm-1
491cm-1
258cm-1
203cm-1
ZnAlPO4 Hydrotalcite (2 hour)
551cm-1
438cm-1
246cm-1
198cm-1
ZnAlPO4 Hydrotalcite (1 hour)
551cm-1
489cm-1
260cm-1
204cm-1
ZnAlPO4 Hydrotalcite (0.5 hour)
551cm-1
491cm-1
251cm-1
200cm-1
Relative Intensity
680
580
480
380
280
180
Wavenumber /cm-1

Figure 7